Received: 5 November 2019 | Accepted: 23 November 2019

DOI: 10.1002/maco.201911357

ARTICLE

Materials and Corrosion

The effect of microstructure on hydrogen permeability of high strength steels

Darya Rudomilova[1] | Tomáš Prošek[1] | Pavel Salvetr[2] | Anna Knaislová[2] | Pavel Novák[2] | Roman Kodým[2] | Gabriela Schimo-Aichhorn[3] | Andreas Muhr[4] | Hubert Duchaczek[4] | Gerald Luckeneder[4]

[1]Department of Metallic Construction Materials, Technopark Kralupy, University of Chemistry and Technology Prague, Kralupy nad Vltavou, Czech Republic

[2]University of Chemistry and Technology Prague, Prague, Czech Republic

[3]CEST Competence Center for Electrochemical Surface Technology, Linz, Austria

[4]voestalpine Stahl GmbH, Linz, Austria

Correspondence
Darya Rudomilova, Department of Metallic Construction Materials, Technopark Kralupy, University of Chemistry and Technology Prague, Žižkova 7, Kralupy nad Vltavou 278 01, Czech Republic.
Email: darya.rudomilova@vscht.cz

Funding information
Grantová Agentura Ceské Republiky, Grant/Award Number: 17-22586S

Abstract

Hydrogen diffusivity and trapping have been studied in two advanced high strength steel grades and model samples using electrochemical permeation test. Microstructures of CP1000 and DP1000 steels consist of ferrite, martensite and a small fraction of retained austenite. In addition, bainite is present in CP1000. Model phases with predominance of a particular phase have been prepared by specific heat treatment. DP1000 has shown the lowest diffusivity among all materials, while ferritic model sample has shown the highest. Differences in hydrogen diffusion coefficient values are linked to trapping microstructural characteristics and grain size.

KEYWORDS

hydrogen-induced cracking, hydrogen permeability, steel

1 | INTRODUCTION

Development and application of advanced high strength steels (AHSSs) is an ever-growing trend in the automotive industry. Broader use of steels with higher strength and good formability instead of conventional steels leads to weight reduction of vehicles and fuel economy. Favourable mechanical properties of AHSSs are achieved by combination of hard and soft phases in their microstructure. For instance, dual phase (DP) AHSSs consists of mostly ferrite and martensite, whereas complex phase (CP) AHSSs contain martensite, tempered martensite, bainite, ferrite and retained austenite.[1,2]

However, AHSSs are susceptible to hydrogen embrittlement (HE) under an applied stress.[3,4] There are a few proposed mechanisms of HE, among which the most accepted theories are hydrogen-enhanced localized plasticity, hydrogen-enhanced strain-induced vacancies, hydrogen-enhanced decohesion or their combinations.[5] A common feature of the theories is that some critical concentration of atomic hydrogen must be reached at a potential crack site and this is achieved by transport of diffusible hydrogen to the regions with higher stress levels. Hence, the diffusible hydrogen can be responsible for hydrogen-induced ductility loss.[6]

When hydrogen is formed on the steel surface during production steps or as a result of corrosion in the service environment, hydrogen diffusion, trapping and detrapping take place inside the material. Hydrogen trapping is characterised by density of trapping sites and their

binding energy. Traps are usually divided into two types: reversible and irreversible trapping sites depending on their binding energy. Despite the fact that some value of energy (60 kJ/mol)[6,7] is being sometimes reported to separate reversible and irreversible trapping sites, their properties form a continuum in view of the binding energy and the probability of hydrogen release. Furthermore, reversible character of trapping sites is dependent on the temperature and increases with increasing temperature.[8] Hydrogen in interstitial lattice sites is diffusible at room temperature and hydrogen released from reversible trapping sites becomes diffusible too. Transport of diffusible hydrogen takes place by interstitial jumps in the lattice, short circuit paths as grain boundaries or by moving dislocations.[9] When hydrogen is trapped in trapping sites with high trap activation energy (irreversible traps) as nonmetallic inclusions and precipitates or high-angle grain boundaries, there is a low probability for hydrogen detrapping from these sites. On the other hand, trapping sites with lower energy as dislocations, low-angle grain boundaries or microvoids can release hydrogen, so they act as both hydrogen sources and sinks. Trapping site density is significantly influenced by microstructure due to varying concentrations of structural defects in different microstructure constituents.

High amount of reversibly trapped hydrogen can lead to the fracture stress decrease and to the change of the fracture behaviour.[10,11] The unfavourable situation can occur during straining, when hydrogen might be rapidly released from these trapping sites to the lattice and diffuse to the high stress fields causing crack initiation.[12] Dislocations can be considered as the most dangerous trapping sites due to their lowest binding energy among other trapping sites.[13] Since the material's susceptibility to HE increases with the reversible trapping site density, it is important to be able to estimate it.

Study of hydrogen diffusion and trapping in AHSSs is very complex issue due to complex microstructures of these steels. Whereas electrochemical permeation test (EPT) was already carried out on different types on AHSSs linking microstructural parameters with hydrogen diffusivity, there are still many questions for further research.[14,15] Winzer et al.[16] reported hydrogen trapping at ferrite/martensite grain boundaries in CP and DP steels. Hadžipašić et al.[17] highlighted the role of dislocations and ferrite/martensite grain boundaries as reversible trapping sites in DP steel. It was shown by Venezuela et al.[18] that hydrogen diffusion coefficient decreases with an increasing amount of martensite in martensitic AHSSs due to a higher dislocation density.[18] Moli-Sanchez et al.[19] demonstrated that enhanced reversible trapping by dislocations in tempered martensitic AHSSs leads to decreasing hydrogen diffusivity and increasing concentration of diffusible hydrogen. Pang et al.[20] explained a lower hydrogen diffusion coefficient in DP steel compared to interstitial free steel by a more complex microstructure with a higher density of phase interfaces, lath boundaries and dislocations. Hydrogen trapping by retained austenite present in most AHSSs was documented in the work of Sojka et al.,[21] who observed that diffusion coefficient decreased with the content of retained austenite in transformation-induced plasticity steels. Zhou et al.[22] showed that trapping binding energy of retained austenite grains changed as a function of the morphology from strong reversible to irreversible.

In this study, two grades of AHSSs were studied in terms of their diffusion and trapping parameters using EPT. To evaluate diffusivity of each microstructure constituent separately, five model structures with the prevalence of one of the phases were prepared and assessed by means of EPT as well. Diffusion coefficients and trap density values obtained for the investigated materials were compared in view of their microstructure.

2 | EXPERIMENTAL

2.1 | Materials

Two grades of AHSSs were used in this study. Samples of CP1000 and DP1000 with ultimate tensile strength Rm 980 MPa were provided by voestalpine Stahl. Both grades contain ~0.2 wt% carbon, ~2.2 wt% manganese, ~1–1.4 wt% chromium and a small amount of niobium and titanium.

Simplified model structures with prevalence of one of the phases were prepared by specific heat treatment of CP1000. CP1000 was used as raw material for production of model phases to avoid influence of changing chemical composition. Different heat treatment procedures were tested to choose optimum conditions for preparation of dense and minimally deformed samples with desired microstructures. Parameters of the finally used heat treatment procedures are described in Table 1. Samples with coarser microstructure (CPF_CM and CPM_CM) were prepared by austenitizing at higher temperatures and/or for longer times.

Phase analysis of CP1000 and DP1000 steels and model samples was performed using X-ray diffraction and neutron diffraction. Microstructure of the steels was studied with scanning electron microscopy (SEM) and light optical microscopy (LOM) after polishing and Nital (3 ml nitric acid and 97 ml ethanol) etching. Phase

TABLE 1 Heat treatment parameters for preparation of model structures

Denomination	Structure with prevalence of	Heat treatment
CPF	Ferrite	1. Annealing at 950°C for 30 minutes 2. Cooling in furnace
CPF_CM	Ferrite	1. Annealing at 1,050°C for 60 minutes 2. Cooling in furnace
CPM	Martensite	1. Annealing at 1,050°C for 30 minutes 2. Cooling in NaCl solution 3. Cooling in liquid nitrogen
CPM_CM	Martensite	1. Annealing at 1,050°C for 60 minutes 2. Cooling in NaCl solution 3. Cooling in liquid nitrogen

fractions and interface areas were determined using image analysis software ImageJ. To determine the prior austenite grain size, samples were polished, over-etched and polished again. Images obtained by LOM revealing prior austenite constituents were analysed by the means of image analysis software ImageJ.

2.2 | Sample preparation

Steel samples were ground down to 1200-grade emery paper, degreased and coated by Pd on one side. The necessity of coating steel with Pd for detection of hydrogen exiting at the anodic side was demonstrated by Manolatos et al.[23] The procedure described in the reference was employed to obtain a well adherent Pd coating.[24] Samples were quickly cleaned in 35 wt% HCl just before application of the coating. The plating solution contained 5 g/L $PdCl_2$ dissolved in 25 wt% ammonia solution. Cathodic current density of 2 mA/cm^2 was applied to the sample for 3 min. The electrochemical plating was followed by heating the sample at 200°C for an hour to release hydrogen absorbed during the electroplating process. The opposite side of the sample was ground using 1200-grade emery paper again just before the start of the permeation experiment.

2.3 | Electrochemical permeation test

The EPT was conducted according to EN ISO 17081 in a double cell originally developed by Devanathan and Stachurski.[25] The used set-up is schematically illustrated in Figure 1. The cell consisted of cathodic and anodic compartments separated by a steel sample. The cathodic part of the cell was filled with 0.5 M sulphuric acid (H_2SO_4) solution with 40 mg/L thiourea (CH_4N_2S) as recombination poison and a cathodic current of 5 to 100 mA/cm^2 was applied between the sample and a platinum counter electrode. The anodic part of the cell contained 0.1 M sodium hydroxide solution. In the anodic part, the Pd-plated side of the sample was polarised to 345 mV against a reference saturated silver/silver chloride electrode immersed into solution using a Luggin capillary. Nitrogen gas was purged through the solution 40 min before and during measurements to prevent steel oxidation. The current between the sample and a platinum counter electrode was measured using a potentiostat BioLogic SP-200.

3 | RESULTS

3.1 | Microstructure characterization

Microstructures of the samples are shown in Figure 2. DP1000 contains approximately 36 vol% ferrite, 62%

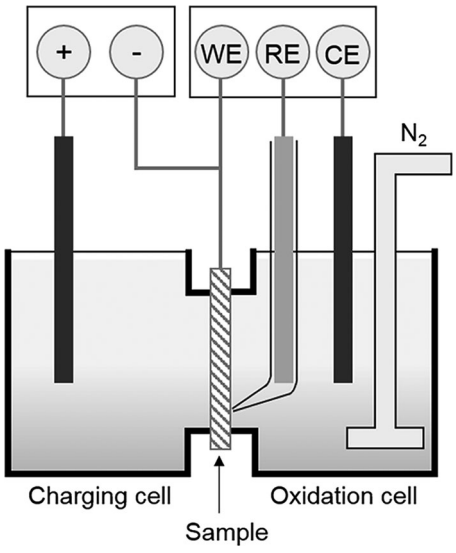

FIGURE 1 Schematic drawing of the used set-up

martensite and 2% retained austenite. Martensite was less etched than ferrite and was present in DP1000 and CP1000 as globular or plate martensite. Martensite forms continuous network in DP1000, while there are individual islands of martensite in CP1000. CP1000 steel contains 32% ferrite, 47% martensite, 20% bainite and 1% retained austenite.

Ferritic model samples CPF and CPF_CM have irregular microstructures with a wide range of ferrite grain sizes. The grains are larger for CPF_CM compared to CPF. Martensitic constituents in CPM_CM are bigger in comparison to CPM. Geometry of the martensite phase is different in model samples and in CP1000 and DP1000. Acicular martensite is present in the model samples, while lath martensite in as-received AHSSs. The difference in martensite morphology may be caused by different amount of carbon in prior austenite phase. The term "grain size" is deliberately avoided for martensitic model structures since martensite is formed by laths and prior austenite grain size should be rather considered. The volume fraction of ferrite, martensite and bainite, prior austenite grain size and interface area are presented in Table 2. The prior austenite grain size provides information about the microstructure coarseness. It is obvious that DP1000 and CP1000 have at least two times finer microstructures compared to model samples. The interface area was calculated from SEM microstructure photographs using software ImageJ. This parameter can be used for comparison of complex microstructures, as it includes not only grain boundaries but also laths interfaces in martensite and bainite. DP1000 and CPM_CM have the highest fraction of phase interfaces in the microstructure, while ferritic model samples have the lowest.

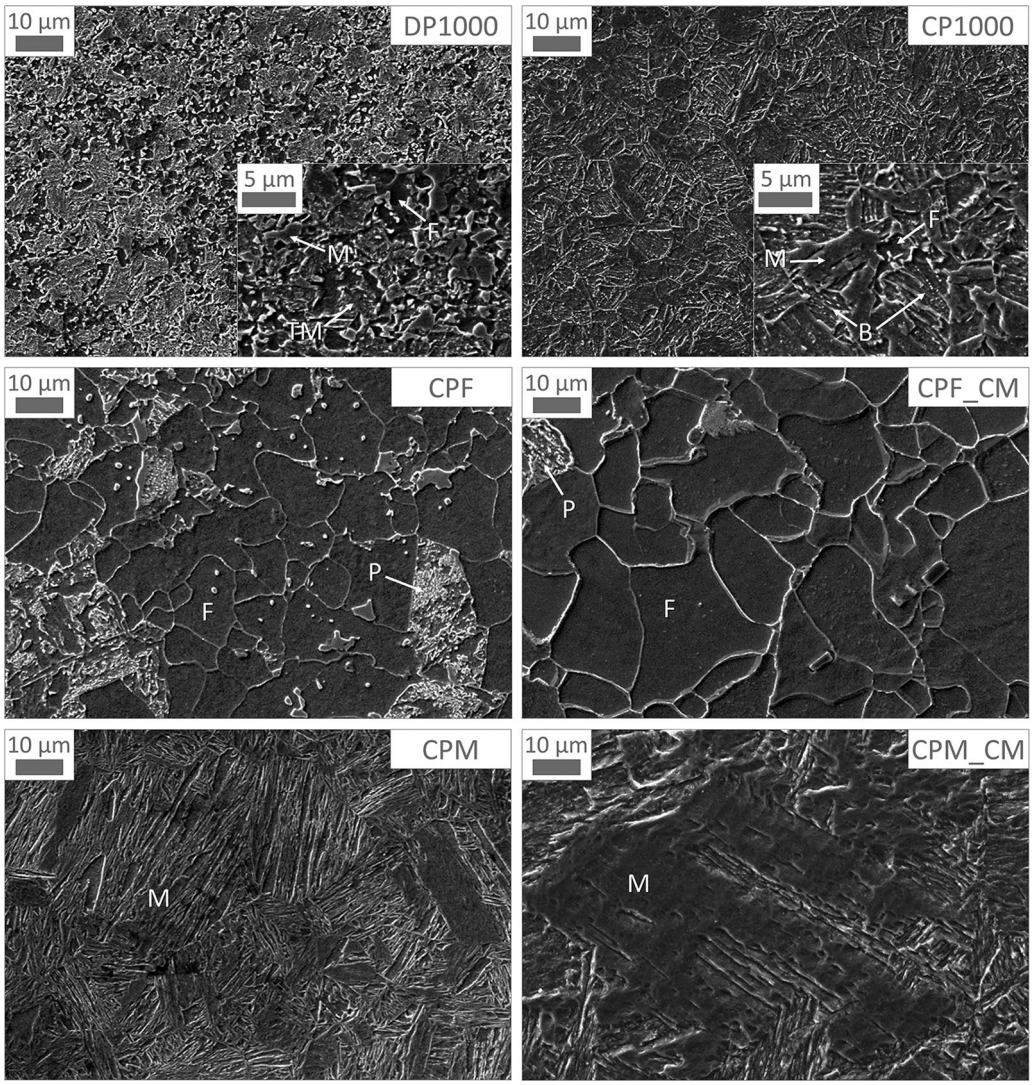

FIGURE 2 Microstructure of CP1000 and DP1000 advanced high strength steels and model samples of CPF (ferritic model structure), CPF_CM (ferritic model structure with coarser microstructure), CPM (martensitic model structure) and CPM_CM (martensitic model structure with coarser microstructure)

TABLE 2 Comparative characteristics of microstructure of studied materials

Denomination	Martensite fraction (%)	Ferrite fraction (%)	Bainite fraction (%)	Prior austenite grain size (μm)	Interface area (%)
DP1000	62 ± 3	36 ± 3		10.0 ± 1.4	16.9 ± 0.3
CP1000	47 ± 2	32 ± 3	20 ± 3	9.1 ± 2.3	13.3 ± 1.1
CPF		73 ± 3		29.4 ± 6.8	7.6 ± 0.7
CPF_CM		93 ± 6		42.2 ± 11.0	10.3 ± 1.1
CPM	87 ± 2			18.6 ± 3.3	14.8 ± 1.2
CPM_CM	95 ± 5			36.1 ± 8.2	18.0 ± 3.8

3.2 | Hydrogen permeability

EPT measurements were carried out for CP1000 and DP1000 AHSSs and five model materials. Hydrogen diffusion coefficients were evaluated from permeation curves by fitting of experimental transient curves with theoretical curves expressed by the following equation for build-up transient:

$$i_t = i_0 + \left(i_\infty - i_0\right)\frac{2L}{\sqrt{\pi D t}}\sum_{n=0}^{\infty}\exp\left(-\frac{(2n+1)^2L^2}{4Dt}\right), \quad (1)$$

where i_t is the measured permeation current density at time t, i_0 is the initial permeation current density, i_∞ is the steady-state permeation current density, L is thickness of the sample and D is hydrogen diffusion coefficient.

Hydrogen permeation transients were measured at different cathodic current densities for all samples. Figure 3 presents a permeation curve for five cathodic charging current densities of 10, 0, 5, 50 and 100 mA/cm^2 applied on the hydrogen entry side of a DP1000 sample. It shows that small current densities did not influence the diffusion coefficient value. However, in the case of the highest current density of 100 mA/cm^2, the diffusion rate increased. It can be linked to more hydrogen produced on the hydrogen entry side and lower influence of hydrogen trapping as most of trapping sites were filled during the previous partial transients. It is in accordance with observations of Liu et al.[26] They reported increasing diffusivity at more negative cathodic polarization potential that is similar in the effect to the case of higher charging current density. The diffusion coefficient obtained at the most negative potential was considered as the lattice diffusion coefficient due to a minimal effect of trapping. In this study, the highest values of hydrogen diffusion coefficient were measured under charging at the highest current density of 100 mA/cm^2.

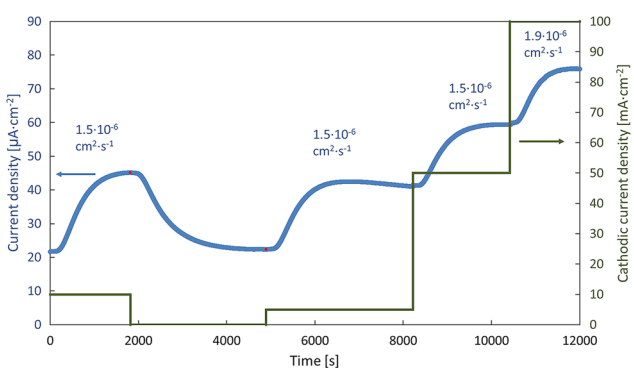

FIGURE 3 Hydrogen permeation transients at different cathodic current densities for DP1000; obtained diffusion coefficient values are given for each transient [Color figure can be viewed at wileyonlinelibrary.com]

Subsequent build-up and decay transients were measured by turning on and off cathodic polarisation of the entry side at 10 mA/cm^2 current density. Permeation transients at 10 mA/cm^2 current density were chosen for comparison of diffusion coefficients assuming better reproducibility of results in comparison with lower current densities. Figure 4 shows examples of typical subsequent build-up and decay transients for DP1000 steel. It indicates that irreversible trapping sites had no significant influence on the hydrogen permeation in this case. Some limited irreversible trapping can be noticed comparing the first and following build-up curves that show a small difference and corresponding slight increase in diffusion coefficient values. However, this effect was small for all steels. Irreversible traps found in AHSSs by other researches were inclusions as MnS.[1,17] Diffusion coefficients evaluated from build-up and decay transients were also close to identical. This proves that trapping and detrapping took place at reversible trapping sites while there was a relatively low number of irreversible traps.

Plots in Figure 5 demonstrate differences in the average values of hydrogen diffusion coefficients measured at 10 mA/cm^2 cathodic current density. These values were calculated from measurements on at least five samples of each material from three subsequent decay transients for each sample. The diffusion coefficients are presented together with respective standard deviations. Diffusion

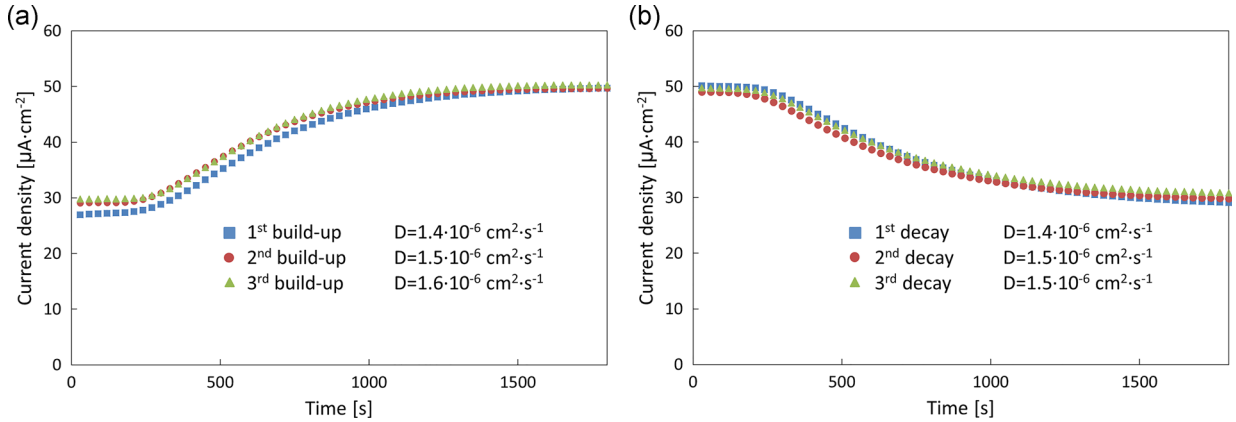

FIGURE 4 Subsequent build-up (a) and decay (b) transients measured for DP1000 at 10 mA/cm^2 cathodic current density [Color figure can be viewed at wileyonlinelibrary.com]

coefficient of CP1000 was approximately two times higher than that of DP1000. The maximal value of diffusion coefficient was measured for ferrite model sample with the coarser microstructure. Diffusivity of martensite model samples was higher compared to CP1000 and DP1000. A significant increase in diffusion rate was observed for the sample with the coarser martensitic microstructure. Comparison of diffusion coefficient values and prior austenite size (Figure 6) suggests that there was a connection between them. The prior austenite grain size can be nominally considered as grain size of the materials. Diffusion coefficient increased with increasing grain size. Another microstructure parameter, the interface area, which is a measure of the relative area of all phase interfaces including laths/matrix boundaries of bainite and martensite, also showed some correlation with hydrogen diffusion coefficient. DP1000 with one of the greatest fraction of the interface area has the lowest hydrogen diffusion coefficient, while the ferrite model samples show the lowest interface area and the highest hydrogen diffusivity.

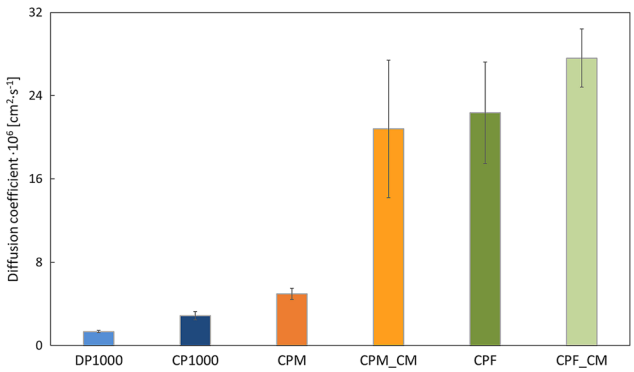

FIGURE 5 Diffusion coefficients for DP1000, CP1000, martensitic (CPM), martensitic with coarser microstructure (CPM_CM), ferritic (CPF) and ferritic with coarser microstructure (CPF_CM) model samples [Color figure can be viewed at wileyonlinelibrary.com]

3.3 | Reversible trapping site density

Reversible trapping site density can be determined using complete decay transient, as it is sensitive to hydrogen detrapping.[27] It was calculated from the area difference between measured decay curve and theoretical curve adjusted using the lattice diffusion coefficient (see Figure 7). Diffusion coefficient obtained from partial build-up at the highest cathodic current density was used as the lattice diffusion coefficient. Calculations of reversible traps density were done in MatLab software using the following equation:

$$N_t = \frac{2A \times 6.24 \times 10^{18}}{L}, \tag{2}$$

where N_t is reversible traps density, A is the area difference between the measured decay transient curve and the theoretical one, L is the sample thickness.[28]

Obtained results presented in Figure 8 show that reversible trap density values grow in the order from CPF to DP1000, which is opposite to the order of diffusion coefficient values. It is in accordance with the

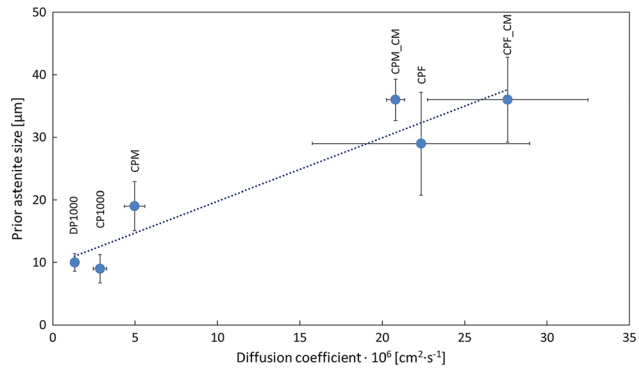

FIGURE 6 Diffusion coefficients compared with values of prior austenite size [Color figure can be viewed at wileyonlinelibrary.com]

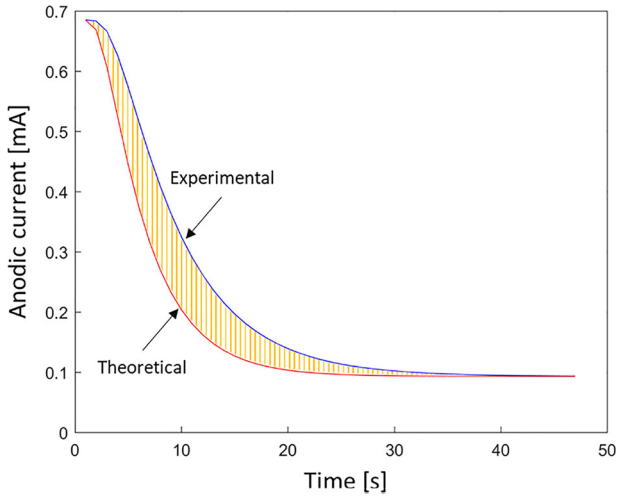

FIGURE 7 Area difference between the measured permeation curve and the theoretical curve calculated with the lattice diffusion coefficient [Color figure can be viewed at wileyonlinelibrary.com]

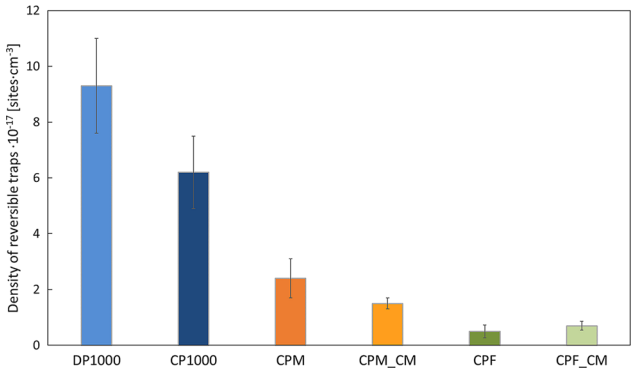

FIGURE 8 Density of reversible trapping sites for DP1000, CP1000, martensitic (CPM), martensitic with coarser microstructure (CPM_CM), ferritic (CPF) and ferritic with coarser microstructure (CPF_CM) model samples [Color figure can be viewed at wileyonlinelibrary.com]

assumption that the material showing the lowest hydrogen diffusivity (DP1000) has the highest density of reversible trapping sites.

4 | DISCUSSION

EPT results allow for calculation of two important parameters in view of HE: hydrogen diffusion coefficient and reversible trapping sites density. It was shown that hydrogen diffusion in DP1000 was two times slower than in CP1000, while reversible trapping site density was 50% higher in DP1000. Prepared model samples with prevalence of ferrite and martensite were used to find correlation between diffusion parameters and the steel microstructure.

The highest diffusion coefficient was measured in the ferrite model samples indicating low hydrogen trapping. However, trapping sites are still present in CPF assuming that diffusion coefficient in well-annealed pure iron with the minimal trapping effect may reach much higher value in order of 10^{-4} $cm^2 \cdot s^{-1}$.[29] Diffusion coefficient of hydrogen in steel may increase with increasing ferrite content due to high hydrogen diffusivity in it. Liu et al.[7] reported that even a small difference in the ferrite content can lead to a noticeable difference in hydrogen diffusion coefficient. Diffusion coefficients for DP980 steel with growing ferrite content increased significantly. It was 0.75×10^{-6}, 1.58×10^{-6} and 2.07×10^{-6} $cm^2 \cdot s^{-1}$ for steels containing 36, 37 and 40 vol% of ferrite, respectively. In parallel, the grain size increased by a factor of 2 and 3 compared to the material with 36% ferrite. However, in our case, DP1000 with the lower hydrogen permeability contained slightly more ferrite than CP1000, 36% and 32%, respectively.

Martensite model samples showed hydrogen diffusion coefficient five times lower than for the ferrite model sample. This is in good agreement with other works. Martensite was reported to significantly affect the permeation rate.[6,18] High hydrogen solubility and low diffusivity in martensitic steels was linked to a large network of dislocations and interfaces between martensite laths.[30] A high trapping effect of interfaces between retained austenite and martensite was also demonstrated.[31] Bainite is present in CP1000 and can also affect hydrogen diffusivity. Depover et al.[32] and Park et al.[33] reported lower hydrogen diffusion coefficients in steels with higher amounts of bainite. This was attributed to high concentration of reversible traps, that is, dislocations and bainite lath boundaries. Hydrogen can be reversibly trapped by cementite present in the bainite and the morphology and size of the iron carbides affect hydrogen diffusivity.[34]

Diffusion coefficient may also be influenced by the content of retained austenite, which is known for its high hydrogen solubility and retarding effect on hydrogen diffusion.[35] Gu et al.[36] proved that hydrogen diffusivity dropped with an increasing fraction of retained austenite. DP1000 and CP1000 contain near the identical content of retained austenite, 2% and 1%, respectively. It can be assumed that the slightly lower amount of austenite might partially explain the higher diffusion coefficient in CP1000, but another contribution to the observed effects is still probable. It is supported by the fact that all model materials irrespective to the prevailing phase showed higher diffusion rate for hydrogen than the as-received CP1000 steel.

The other aspect that should be considered is the grain boundary and interface area. Grain boundaries can work as "pipelines" for hydrogen due to a large vacancy density.[37] In parallel, they can serve as traps. The trapping effect of grain boundaries can be linked to the presence of triple junctions and dense precipitates.[38,39] Accumulation of hydrogen along grain boundaries was experimentally observed by Koyama et al.[40] by means of silver decoration technique. Yazdipour et al.[38] reported that diffusion coefficient grows with increasing grain size and there is some intermediate grain size (46 μm) corresponding to the highest diffusivity. Hydrogen diffusion becomes slower with further coarsening due to decrease in the grain boundary area fracture. This observation was attributed to the competition between the trapping effect of triple junctions and enhanced mobility of hydrogen along grain boundaries. In the present work, grain size of the ferrite sample with coarser microstructure did not reach this critical value, thus hydrogen diffusion coefficient was still growing in the order CP1000-CPF-CPF_CM. López-Martínez et al.[41] also observed that larger grains and smaller grain boundary area led to fewer diffusion paths and as a result to lower diffusion coefficients in steel. On the other side, Stopher et al.[42] reported that the amount of trapping sites increased with decreasing grain size. Lan et al.[43] and Haq et al.[44] showed that coarsening of a steel matrix microstructure led to an increase of hydrogen diffusion coefficient. These studies seem to correspond to results obtained in our measurements, where all model structures have coarser microstructures compared to CP1000 and DP1000 steels and revealed higher hydrogen diffusion rates. Furthermore, diffusion coefficients in model samples with coarser microstructures (CPF_CM and CPM_CM) were higher than in model samples CPF and CPM (see Figures 5 and 6).

However, the situation is complicated in the case of model samples with prevailing martensite and the AHSSs as not only prior austenite grain boundaries but all interfaces including lath/matrix boundaries should be taken into account. Rehrl et al.[2] associated higher diffusivity measured for DP1200 with less interfaces, that is, phase and grain boundaries, compared to CP1200 and CP1400. In this study, one of the largest interface area was revealed in DP1000, which is in agreement with the lowest diffusivity among the studied materials. However, the same correlation does not apply for martensite and ferrite model samples. It should be noted that certain inaccuracy in the determination of the interface area fraction is possible. The reason for it is that the interface area was obtained by image analysis of SEM micrographs where not all martensite laths can be visible as every lath consists of further smaller laths. It is also possible that a part of interfaces in DP1000 and CP1000 were undetected due to their very fine-grained microstructure. It can be expected that for the ferrite model samples, the interface area most likely corresponds to the grain boundary area. Thus, there is a correlation between diffusion coefficient and grain size as well.

Hydrogen trapping should be discussed in view of all possible trapping sites: grain boundaries, lath boundaries, precipitates and dislocations.[45] The results presented in Figure 8 show stronger hydrogen trapping in DP1000 and CP1000 compared to the model samples. It can be associated with more complex microstructure of the AHSSs. Trapping between grains of different phases can play a very significant role as it was demonstrated for ferrite/martensite, martensite/austenite and ferrite/austenite interfaces.[16,22] It is also possible that CP1000 and DP1000 contain more precipitates working as reversible trapping sites. Micro-alloying elements are added to AHSSs to produce very fine-grained microstructure with numerous small precipitates for improved strengthening effect.[46] Despite the fact that model phases contain the same amount of alloying elements as CP1000, it is possible that a part of them stayed dissolved in the matrix after the additional heat treatment. Consequently, model samples revealed coarser microstructures indicating that micro-alloying elements retarded grain growth insufficiently. The other possible reason for higher trapping density in as-received materials is larger dislocation density. Annealing step during preparation of model samples from CP1000 sheets could decrease a number of dislocations and cause higher hydrogen diffusivity and lower trap density in all model samples.

5 | CONCLUSION

Hydrogen diffusion coefficients in AHSSs and model structures were measured using electrochemical permeation test. DP1000 revealed the lowest hydrogen diffusion coefficient and the highest density of trapping sites. Significantly higher diffusion coefficient was measured for model structures. The ferrite model sample with the coarser microstructure was the most permeable for hydrogen. Two reasons related to the sample microstructure were identified to increase hydrogen diffusion: larger grain size and smaller amount of interfaces beneficial for hydrogen trapping. Other factors, such as a lower amount of precipitates and lower dislocations density, can also play a role. The effect of irreversible trapping sites on hydrogen transport was found to be insignificant for the studied materials.

ACKNOWLEDGEMENT

A part of this study was financially supported by the Czech Science Foundation, project No. 17-22586S.

ORCID

Darya Rudomilova http://orcid.org/0000-0002-9269-2803

REFERENCES

[1] J. Rehrl, K. Mraczek, A. Pichler, E. Werner, *Mater. Sci. Eng., A* **2014**, *590*, 360.
[2] J. Rehrl, K. Mraczek, A. Pichler, E. Werner, *Steel Res. Int.* **2014**, *85*, 336.
[3] N. Eliaz, A. Shachar, B. Tal, D. Eliezer, *Eng. Fail. Anal.* **2002**, *9*, 167.
[4] Y. H. Liu, X. H. Jin, J. M. Hu, M. Zhang, J. Wang, A. Atrens, *Corros. Rev.* **2016**, *34*, 127.
[5] M. Koyama, C. C. Tasan, E. Akiyama, K. Tsuzaki, D. Raabe, *Acta Mater.* **2014**, *70*, 174.
[6] M. I. Luppo, J. Ovejero-Garcia, *Corros. Sci.* **1991**, *32*, 1125.
[7] Q. Liu, J. Venezuela, M. Zhang, Q. Zhou, A. Atrens, *Corros. Sci.* **2016**, *111*, 770.
[8] G. M. Pressouyre, *Metal. Mater. Trans. A* **1979**, *10*, 1571.
[9] G. M. Pressouyre, *Acta Metall. Mater.* **1980**, *28*, 895.
[10] M. Loidl, O. Kolk, S. Veith, T. Göbel, *Materialwiss. Werkst.* **2011**, *42*, 1105.
[11] M. Wang, E. Akiyama, K. Tsuzaki, *Corros. Sci.* **2007**, *49*, 4081.
[12] J. Ćwiek, *J. Mater. Process. Tech.* **2005**, *164*, 1007.
[13] E. I. Galindo-Nava, B. I. Y. Basha, P. E. J. Rivera-Díaz-del-Castillo, *J. Mater. Sci. Technol.* **2017**, *33*, 1433.
[14] D. Rudomilova, T. Prošek, G. Luckeneder, *Corros. Rev.* **2018**, *36*, 413.
[15] D. Rudomilova, T. Petrek, T. Prošek, V. Šefl, H. Duchaczek, F. Zwettler, A. Muhr, G. Luckeneder, *Mater. Corros.* **2018**, *69*, 1398.
[16] N. Winzer, O. Rott, R. Thiessen, I. Thomas, K. Mraczek, T. Höche, L. Wright, M. Mrovec, *Mater. Design* **2016**, *92*, 450.
[17] A. B. Hadžipašić, J. Malina, M. Malina, *Chem. Biochem. Eng. Q.* **2011**, *25*, 159.
[18] J. Venezuela, Q. Zhou, Q. Liu, M. Zhang, A. Atrens, *Adv. Eng. Mater.* **2018**, *20*, 1700468.
[19] L. Moli-Sanchez, F. Martin, E. Leunis, J. Chêne, M. Wery, *Defect Diffus. Forum* **2012**, *323-325*, 485.
[20] X. Pang, F. Fazeli, M. Attard, C. Shi, *Mater. Sci. Forum* **2014**, *783-786*, 950.
[21] J. Sojka, P. Štepán, P. Vánová, presented at *Metal 2013: 22nd Int. Conf. Metall. Mater.*, Brno, Czech Republic, 15 – 17 May, **2013**, p. 626.
[22] P. Zhou, W. Li, H. Zhao, X. Jin, *Int. J. Hydrogen Energ.* **2018**, *43*, 10905.
[23] P. Manolatos, M. Jerome, J. Galland, *Electrochim. Acta* **1995**, *40*, 867.
[24] P. Manolatos, M. Jerome, *Electrochim. Acta* **1996**, *41*, 359.
[25] M. A. V. Devanathan, Z. Stachurski, *P. Roy. Soc. Lond. A. Mat.* **1962**, *270*, 90.
[26] Q. Liu, A. D. Atrens, Z. Shi, K. Verbeken, A. Atrens, *Corros. Sci.* **2014**, *87*, 239.
[27] T. Zakroczymski, *Electrochim. Acta* **2006**, *51*, 2261.
[28] Q. Liu, A. Atrens, *Corros. Sci.* **2015**, *96*, 112.
[29] H. J. Grabke, E. Riecke, *Mater. Tehnol.* **2000**, *34*, 331.
[30] S. L. I. Chan, *J. Chin. Inst. Eng.* **1999**, *22*, 43.
[31] S. L. I. Chan, H. L. Lee, J. R. Yang, *Metall. Trans. A* **1991**, *22*, 2579.
[32] T. Depover, E. V. den Eeckhout, K. Verbeken, *Mater. Sci. Tech. Ser.* **1625**, *2016*, 32.
[33] J. H. Park, M. Oh, S. J. Kim, *J. Mater. Res.* **2017**, *32*, 1295.
[34] V. P. Ramunni, T. D. P. Coelho, P. E. V. de Miranda, *Mat. Sci. Eng. A-Struct.* **2006**, *435*, 504.
[35] L. C. D. Fielding, E. J. Song, D. K. Han, H. K. D. H. Bhadeshia, D. W. Suh, *Proc. R. Soc. Lond. A. Mat.* **2014**, *470*, 20140108
[36] Y. Gu, S. Zeng, P. Qiu, Y. Wu, D. Peng, *J. Iron Steel Res. Int.* **2004**, *11*, 42.
[37] C. Park, N. Kang, S. Liu, *Corros. Sci.* **2017**, *128*, 33.
[38] N. Yazdipour, A. J. Haq, K. Muzaka, E. V. Pereloma, *Comp. Mater. Sci.* **2012**, *56*, 49.
[39] L. W. Tsay, H. L. Lu, C. Chen, *Corros. Sci.* **2008**, *50*, 2506.
[40] M. Koyama, D. Yamasaki, T. Nagashima, C. C. Tasan, K. Tsuzaki, *Scripta Mater.* **2017**, *129*, 48.
[41] E. López Martínez, H. J. Vergara Hernández, O. Flores, B. Campillo, *ISIJ Int.* **2015**, *55*, 2435.
[42] M. A. Stopher, P. Lang, E. Kozeschnik, P. E. J. Rivera-Diaz-del-Castillo, *Mater. Design* **2016**, *106*, 205.
[43] L. Lan, X. Kong, Z. Hu, C. Qiu, D. Zhao, L. Du, *Corros. Sci.* **2016**, *112*, 180.
[44] A. J. Haq, K. Muzaka, D. P. Dunne, A. Calka, E. V. Pereloma, *Int. J. Hydrogen Energ.* **2013**, *38*, 2544.
[45] S. Frappart, X. Feaugas, J. Creus, F. Thebault, L. Delattre, H. Marchebois, *J. Phys. Chem. Solids* **2010**, *71*, 1467.
[46] W. Bleck, K. Phiu-on, presented at *Joint Int. Conf. HSLA Steels 2005 ISUGS 2005*, Sanya, China, 8 – 10 November, **2005**, p. 50.

How to cite this article: Rudomilova D, Prošek T, Salvetr P, et al. The effect of microstructure on hydrogen permeability of high strength steels. *Materials and Corrosion*. 2020;71:909–917. https://doi.org/10.1002/maco.201911357